EasyChair Preprint

№ 5121

Measurements and CFD Modeling of Outdoor Radon Dispersion

Rabi Rabi, Lhoucine Oufni, Elhoucine Youssoufi,
Khamiss Cheikh, Hamza Badry and Youssef Errami

March 9, 2021

Measurements and CFD modeling of outdoor radon dispersion

Rabi RABI
Materials Physics Laboratory
Department of Physics
Faculty of Sciences and Techniques
Sultan Moulay Slimane University
Béni Mellal, Morocco
rabiismcm@gmail.com

Lhoucine OUFNI*
Materials Physics Laboratory
Department of Physics
Faculty of Sciences and Techniques Sultan Moulay Slimane University
Béni Mellal, Morocco
oufni@usms.ma

Elhoucine YOUSSOUFI
Materials Physics Laboratory
Department of Physics
Faculty of Sciences and Techniques
Sultan Moulay Slimane University
Béni Mellal, Morocco
Youssoufielhoucine21@gmail.com

Khamiss CHEIKH
Electronic Instrumentation and Energy Laboratory
Department of Physic
Faculty of Sciences Chouaib Doukkali University
El Jadida, Morocco
cheikhkhamiss@gmail.com

Hamza BADRY
Materials Physics Laboratory
Department of Physics
Faculty of Sciences and Techniques
Sultan Moulay Slimane University
Béni Mellal, Morocco
badryh@gmail.com

Youssef ERRAMI
Electronic Instrumentation and Energy Laboratory
Department of Physic
Faculty of Sciences Chouaib Doukkali University
El Jadida, Morocco
errami.emi@gmail.com

***Abstract* — Inhalation of radon (^{222}Rn) and its daughter product are a major source of natural radiation exposure. The measurement and numerical modeling of radon concentration in outdoor is assuming ever increasing importance. It is known from recent surveys in many countries that radon and its progeny contribute significantly to total inhalation dose and it is fairly established that radon when inhaled in large quantity causes lung disorder. Keeping this in view, this study focuses on investigating both numerically and experimentally the influence of geological and meteorological conditions on the radon concentration outdoor. The numerical results showed that ventilation rate, temperature and humidity have significant impacts on both radon content and distribution. The variations of radon concentration with the ventilation, temperature and relative humidity are discussed. The numerical simulation results were validated with analytical calculation and experimental measurement. The experimental measurement was performed using Radon Scout PLUS. The simulation and analytical calculation in this study are relatively consistent to the measurement results.**

Keywords: Radon, SSNTD, Exhalation rate, Computational Fluid Dynamics (CFD), Measurement method, Analytical method.

I.INTRODUCTION

^{222}Rn a decay product of ^{226}Ra in the naturally occurring ^{238}U series is a radioactive inert gas and constitutes about half the radiation dose received by general inhabitants. The quantity of ^{222}Rn that emitted from the ground surface depends mainly on the amounts of ^{226}Ra present in the area and also the type of the soil and its porosity. Radon and its short-lived decay products can be deposited in the lung tissues and give rise to elevated radiation doses. Long time exposure of people to higher concentrations of radon and its progeny may lead to lung cancer and other pathological effects such as respiratory functional changes [1]. Health effects of radon, most notably lung cancer, have been studied for several decades. Radon is now recognized as the second most important cause of lung cancer after smoking in the general population [2, 3].

The radon exhalation rate from the ground surface depends on the geological factors such as porosity, temperature difference between top layers of soil, moisture content and permeability of the soil. Meteorological factors such as rainfall, wind speed, atmospheric humidity and atmospheric pressure influence the transport and distribution of radon and its progeny concentrations in the atmosphere [4, 5].

Computational fluid dynamics (CFD) are a very powerful tool for the studies of radionuclides dispersion with the factors considered individually or in combination with the wind field effect [6]. Many CFD based studies have been performed to investigate outdoor radon dispersion [7-11]. The applicability of CFD for radon related research is still evolving and a lot needs to

be done in applying this knowledge for mankind research.

In this study, FLUENT, a CFD software package was used to simulate and visualize the effects of geological and meteorological conditions on the radon concentration outdoor. In addition, the radon exhalation and radium concentration in soil has been measured using solid state nuclear track detectors (SSNTD) technique that is widely used to measure radon, radium and thorium in various samples [12, 13]. This technique has been well documented, and has found wide application [14, 15]. Measurements and analytical calculation were also performed for validation of CFD model.

II. MODELS

A. Mathematical models

In general, ^{222}Rn is emitted from soil, then mixes with the air and disperses in three directions into the atmosphere. The three-dimensional (3D) steady state governing equations for CFD depicting atmospheric wind distributions are described as follows [6].

The continuity equation is given as:

$$\frac{\partial(\rho u_i)}{\partial x_i} = 0 \qquad (1)$$

where x is the coordinate axis in the direction i (i = 0, 1, 2), u_i corresponds to the mean velocity in i direction, and ρ is the air density. The turbulent momentum equation is formulated as:

$$\frac{\partial(\rho u_i u_j)}{\partial x_i} = \frac{-\partial P}{\partial x_i} + \frac{\partial}{\partial x_i}\left[(\mu_t + \mu)\left(\frac{\partial u_i}{\partial x_j} + \frac{\partial u_j}{\partial x_i}\right)\right] + \rho g \qquad (2)$$

where P is pressure, μ_t is the turbulent viscosity, μ is the molecular viscosity, and g is the gravitational acceleration. The turbulence kinetic energy k and the dissipation rate of turbulence kinetic energy ε are thus expressed as [6]:

$$\frac{\partial(\rho u_i k)}{\partial x_i} = \frac{\partial}{\partial x_i}\left[\left(\mu + \frac{\mu_t}{\sigma_k}\right)\frac{\partial k}{\partial x_i}\right] + \mu_t \frac{\partial u_j}{\partial x_i}\left(\frac{\partial u_i}{\partial x_j} + \frac{\partial u_j}{\partial x_i}\right) - \rho\varepsilon \qquad (3)$$

$$\frac{\partial(\rho u_i \varepsilon)}{\partial x_i} = \frac{\partial}{\partial x_i}\left[\left(\mu + \frac{\mu_t}{\sigma_\varepsilon}\right)\frac{\partial \varepsilon}{\partial x_i}\right] + C_{1\varepsilon}\mu_t \frac{\varepsilon}{k}\frac{\partial u_j}{\partial x_i}\left(\frac{\partial u_i}{\partial x_j} + \frac{\partial u_j}{\partial x_i}\right) - \rho C_{2\varepsilon}\frac{\varepsilon^2}{k} \qquad (4)$$

The turbulence viscosity is given as:

$$\mu_t = C_\mu \rho k^2/\varepsilon \qquad (5)$$

where C_μ, $C_{1\varepsilon}$, $C_{2\varepsilon}$, σ_k and σ_ε are empirical and experimental constants fixed as 0.09, 1.44; 1.92; 1.0 and 1.3, respectively [16].

Radon formed in the soil is released into the atmosphere: Radon transport through soils can be described by diffusion-decay processes. After exhalation from soil, the radon is distributed into atmosphere by means of diffusion and convection. Assuming steady-state conditions and including source terms, the equation of radon transport between soil and atmosphere is given as [17]:

$$\frac{\partial(uC)}{\partial x_i} = D_e\left(\frac{\partial^2 C}{\partial {x_i}^2}\right) - \lambda C + \frac{\lambda \rho_s A_{Ra} f}{\epsilon} \qquad (6)$$

where x is the coordinate axis in the direction i (i = 0, 1, 2), D_e is the effective radon diffusion coefficient, C is the radon concentration, λ is the radon decay constant, ϵ is the effective porosity of the soil, ρ_s is the dry bulk density of the soil, A_{Ra} is the radium activity in the soil particles and f is the radon emanation coefficient.

B. Numerical solution and boundary conditions

A CFD software (Fluent) based on the Finite Volume Method has been used to solve the set of equations introduced in the previous section [18]. Rectangular Cartesian grids with 600,000 control volumes are used; the size of the smallest control volumes, placed close to the ground is 0.01 m and a stretching factor of 1.1 is adopted. A sensitivity analysis of the numerical scheme on the grid refinement has been performed by using a finer grid (800,000 volumes), but the change in the results was negligible. The criterion for numerical convergence, i.e., the maximum relative difference between two consecutive iterations was less than 10^{-5}.

As far as the boundary conditions are concerned, at the upwind boundary a logarithmic profile of the stream wise velocity component U is applied [18, 19].

$$U(y) = \frac{u_0}{k}\ln\left(\frac{y}{y_0}\right) \qquad (7)$$

where y is the distance from the ground, k = 0.4187 is the Von Karman's constant, u_0 = 0.183 m s^{-1} and y_0 = 0.0195 m [19].

In addition, as the distribution of k and ε on the inlet boundary is not known, the following relations are used [19]:

$$k(y) = \frac{u_0^2}{\sqrt{c_\mu}} \quad \text{and} \quad \varepsilon(y) = \frac{u_0^3}{k(y + y_0)} \qquad (8)$$

III. FIELD MEASUREMENTS

A. Passive measurement: Measurements of radon activity, radon exhalation rate and radium concentration

The study was performed in peripheral road in Beni-Mellal city. The city is located in the central part of Morocco (32 200 N, 6 210 W) between the High Atlas Mountain and the vast Tadla plain with altitude of 450–600 m and is characterized by a semi-arid climate with averaged annual temperature of 26 °C and annual rainfall of 400 mm.

The measurement method is based on using CR-39 and LR-115 type II solid state nuclear track detectors (SSNTDs) for measuring the radium activity (^{226}Rn) and radon exhalation rate from samples soil. The disk-shaped CR-39 and LR-115 type II solid state nuclear track detectors (SSNTD) have been separately placed in close contact with soil samples in a hermetically sealed cylindrical plastic container for 30 days. During this time, α-particles emitted by the nuclei of the radium and thorium series have bombarded the SSNTD films. After the irradiation, the exposed films were etched in a NaOH solution at optimal conditions of etching, ensuring good sensitivities of the SSNTDs and a good reproducibility of the registered track density rates: 2.5 N solution at 60 °C for 1.5 h for the LR-115 type II films and 6.25 N solution at 70° C for 6 h for the CR-39 detectors. After this chemical treatment, these SSNTDs were washed, dried and scanned using an optical microscope [12, 13].

Under our experimental conditions, and assuming that there is a secular equilibrium between radium, thorium and their daughters, thus knowing the track densities on each SSNTD used, we can evaluate the radium activities by using the following equations:

$$D_G^{LR} = 0.5\,\rho_s\,\Delta R_s \sin^2\theta_c'\,A_c(^{226}\mathrm{Ra})\left[4 + 3\frac{A_c(^{232}\mathrm{Th})}{A_c(^{226}\mathrm{Ra})}\right] \quad (9)$$

$$D_G^{CR} = 0.25\,\rho_s \sin^2\theta_c A_c(^{226}\mathrm{Ra})\left[\sum_{i=1}^{8} k_i R_{\alpha i} + \frac{A_c(^{232}\mathrm{Th})}{A_c(^{226}\mathrm{Ra})}\sum_{i=1}^{7} k_i R_{\alpha i}\right] \quad (10)$$

where D_G^{LR} and D_G^{CR} are the track density rates registered on the LR-115 type II and CR-39 (tracks $cm^{-2}s^{-1}$), $A_c(^{226}\mathrm{Ra})$ and $A_c(^{232}\mathrm{Th})$ are the radium (^{226}Ra) and thorium (^{232}Th) α-activities inside the studied soil samples (Bq kg^{-1}), ρ_s is the soil samples density (kg m^{-3}), k_i is the branching ratio in %, $R_{\alpha i}$ is the range of α-particle of energy $E_{\alpha i}$ and index i inside the soil samples and it is calculated by means of the TRIM program, θ_c and θ_c' are the critical angles of etching for the LR-115 type-II and CR-39, respectively. $\Delta R_s = R_{max} - R_{min}$ where R_{max} and R_{min} are the α-particle ranges in the soil samples which correspond to the lower and upper ends of the energy window which depend on the residual thickness of the LR-115 SSNTD [12,13].

Combining equations (9) and (10), we obtain the following relationship between the radium (^{226}Ra) to thorium (^{232}Th) ratios and track densities. Indeed, we have:

$$\frac{A_c(^{232}\mathrm{Th})}{A_c(^{226}\mathrm{Ra})} = \frac{0.5\sin^2\theta_c\sum_{i=1}^{8} k_i R_{\alpha i} - 4\gamma'\Delta R_s\sin^2\theta_c'}{\left[3\gamma'\Delta R_s\sin^2\theta_c' - 0.5\sin^2\theta_c\sum_{i=1}^{7} k_i R_{\alpha i}\right]} \quad (11)$$

where: $\gamma' = \frac{D_G^{CR}}{D_G^{LR}}$

From where one obtains the radium activity given by:

$$A_c(^{226}\mathrm{Ra}) = \frac{2\,D_G^{LR}}{\Delta R_s\,\rho_s\sin^2\theta_c'\left[4 + 3\frac{A_c(^{232}\mathrm{Th})}{A_c(^{226}\mathrm{Ra})}\right]} \quad (12)$$

For the calculation of radon α-activities, we have placed the SSNTD at a distance of 9 cm above the soil samples. The range for the α-particles emitted by radon and their corresponding daughters in the gas volume has been determined by the TRIM program. The radon α-activities per unit volume have been measured outside [$A_c(^{222}\mathrm{Rn})$] different samples by using the track densities measured on the LR-115 [D^*(LR)] SSNTDs given by [7]:

$$D^*(LR) = \frac{A_c(^{222}\mathrm{Rn})}{4}\sin^2\theta_c[R_{max} - R_{min}] \quad (13)$$

where R_{max} and R_{min} are the ranges of α-particles in the air (gas) volume, $Ac(^{222}\mathrm{Rn})$ is the alpha activity outside soil sample (Bq m^{-3}).

In order to measure the radon exhalation rate the cylindrical plastic container technique was used. The exhalation rate of radon is obtained by [7]:

$$E_0 = \frac{A_c(^{222}\mathrm{Rn})VT\lambda}{A\left[T - \frac{1}{\lambda(1-e^{-\lambda T})}\right]} \quad (14)$$

where E_0 is the radon exhalation rate, $Ac(^{222}\mathrm{Rn})$ is the integrated radon exposure as measured by LR-115 II film, V is the effective volume of the plastic container (m^3), λ is the decay constant for radon, T is the exposure time (h), and A is the area of the plastic container (m^2).

B. Active measurement method

The outside radon concentrations were continuously measured with monitor (Radon Scout PLUS) instrument. It is used to identify problems of outdoor radon and influences of environmental factors such as ventilation

effects, temperature and relative humidity are also measured and logged, so that any influence from the measuring environment can be determined. The technical characteristics of this device are:

- The range of measurement is from 0 to 2 MBq m^{-3};
- The sensitivity is 1.8 cpm (kBq m^{-3})$^{-1}$;
- Linearity error less than 5%.

For measurement, the detector was placed above the ground.

IV. ANALYTICAL METHOD

The radon concentration in the soil is determined using an analytical approach which can be described by the equation [20]:

$$C_{Rn} = \frac{\rho_s A_{Ra} f}{\epsilon} + \left(C_0 - \frac{\rho_s A_{Ra} f}{\epsilon}\right) \exp\left(-\frac{\sqrt{\lambda D_e}}{D_e} y\right) \quad (15)$$

where C_{Rn} is radon concentration in the soil, ρ_s is the dry bulk density of the soil, A_{Ra} is the ^{226}Ra activity in soil particles, f is the radon emanation coefficient, ϵ is the effective porosity of the soil, y is depth in soil , λ is the radon decay constant and D_e is the effective radon diffusion coefficient in soil.

V. RESULTS AND DISCUSSION

The radon activities, radium contents and radon exhalation rates in the soil samples collected from the Beni-Mellal area Morocco, are summarized in Table 1. These results show that the radium content in the studied samples vary from 2.15 to 5.14 Bq Kg^{-1}, the radon exhalation rate varied from 159.14 to 379.78 mBq m^2 h^{-1}, whereas the radon activity varies between 172.11 and 410.72 Bq m^{-3}. From the statistical error on track counting one can determine the error on track density per unit time and then evaluate the relative uncertainty of the radium content and radon activity determination which is about 6%.

To establish the correlation between the radon exhalation rate and the radium content in soil samples depth, variations of radon exhalation rate and radium content with the depth of soil are plotted in Fig. 1. There seems to be a positive correlation between radon exhalation rate and the radium concentration. The linear coefficients are found to be 0.98.

The CFD model described above was used to determine the concentration of radon in the soil. Using the radium concentration in the soil measured above, the porosity and density of soil ($\epsilon = 0.32$, ρ_s = 1.51 g cm^{-3}, respectively), are the key inputs for CFD model.

The results of the vertical distribution of the radon concentration in the soil can be seen in Fig. 2. It can be noticed from this figure the concentration of radon increases with depth, this is due to the concentration of radium which also increases with depth. Model validation was performed using analytical solution from Equation (15). We notice that the comparisons between results of CFD model and analytical method are in unexpected agreement with the experimental data (Fig. 2).

The radon concentration in the soil is larger than in the atmosphere because of the radon production in soil from the radium decay chain. This means that radon diffusion is in the direction of soil to the atmosphere. Once in the atmosphere the radon continues to decay and as a result the concentration decreases with height above ground. The results of CFD model are shown in Fig. 3. The CFD model results of outdoor radon concentration are in agreement with the results of experimental data (Fig. 3).

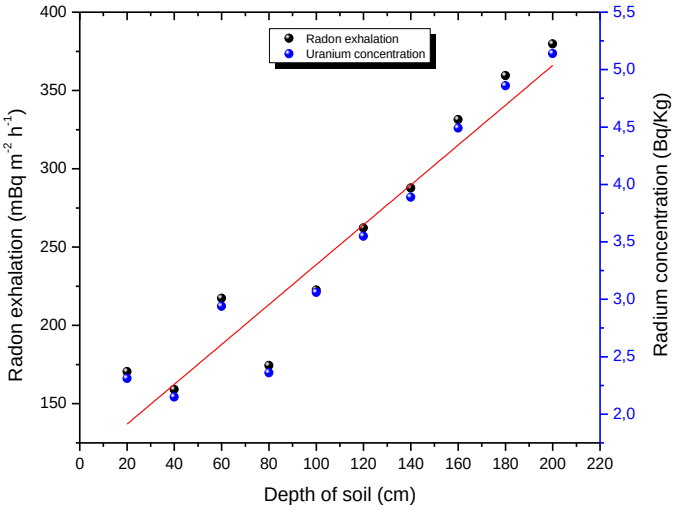

Fig. 1. Radon exhalation rate and radium content vs. the average depth of the soil samples.

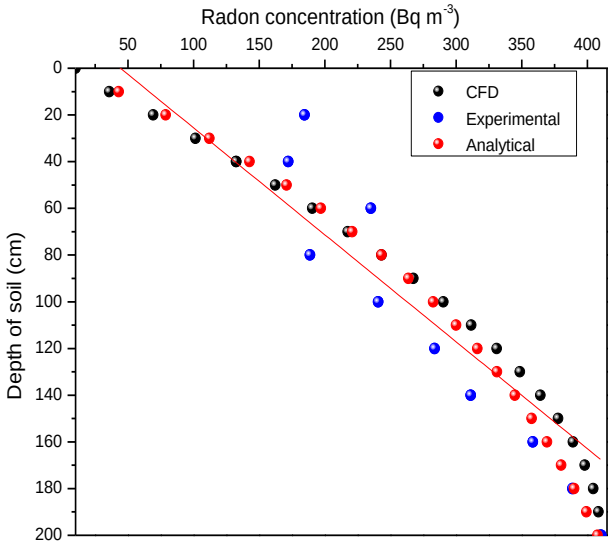

Fig. 2. The concentration of radon outside soil as the function of soil depths.

TABLE I. DATA OBTAINED FOR RADON EXHALATION RATE, RADON ACTIVITY AND RADIUM CONTENT IN VARIOUS STUDIED SOIL SAMPLES.

Depth of soil (cm)	$D_T^{CR} \times 10^3$ (tr $cm^{-2}s^{-1}$)	$D_T^{LR} \times 10^3$ (tr $cm^{-2}s^{-1}$)	Radon concentration (Bq m^{-3})	Radon exhalation rate, mBq $m^{-2}h^{-1}$	Radium concentration, Bq Kg^{-1}
20	1.29±0.06	0.39±0.01	184.45 ± 9.27	170.55± 8.57	2.31±0.15
40	1.21±0.07	0.36±0.02	172.11 ± 10.02	159.14± 9.26	2.15±0.14
60	1.65±0.07	0.49±0.02	235.07 ± 11.20	217.36± 10.35	2.94±0.22
80	1.32±0.06	0.40±0.02	188.64 ± 8.82	174.43± 8.57	2.36±0.17
100	1.69±0.05	0.51±0.02	240.73 ± 10.46	222.60± 9.67	3.06±0.23
120	1.99±0.07	0.60±0.03	283.63 ± 13.32	262.26± 12.31	3.55±0.26
140	2.19±0.06	0.66±0.01	311.21 ± 14.63	287.77± 13.52	3.89±0.36
160	2.52±0.05	0.76±0.03	358.47 ± 17.16	331.47± 15.86	4.49±0.36
180	2.73±0.07	0.82±0.03	388.72 ± 17.36	359.44± 16.05	4.86±0.37
200	2.89±0.07	0.87±0.03	410.72 ± 17.74	379.78± 16.40	5.14±0.42

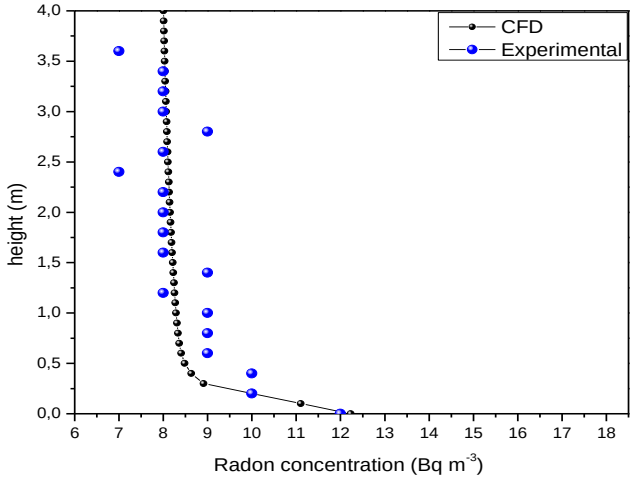

Fig. 3. Vertical distribution of radon concentration in outdoor.

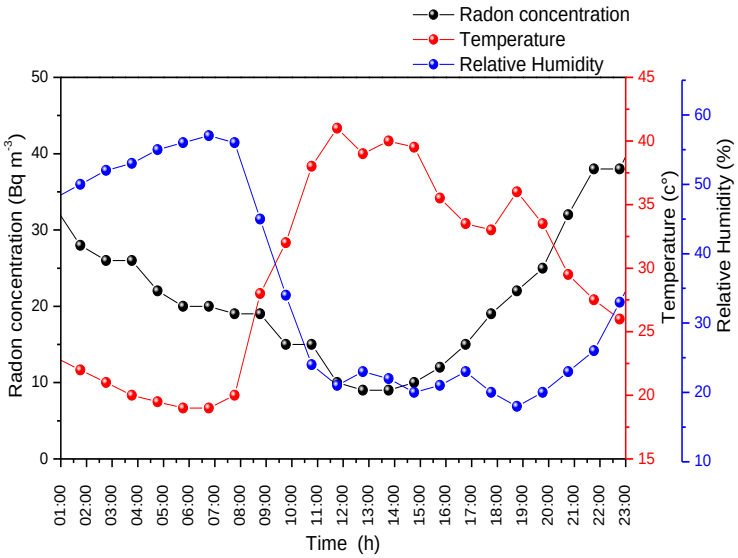

Fig. 4. Hourly concentration of radon in outdoor (Wednesday, May, 2019).

In order to show the effect of meteorological parameters (temperature and humidity) on radon levels, we performed a continuous measurement of radon activity in the open air for one day in May, 2019, the data obtained are shown in Fig. 4. The diurnal variation of the radon concentration shows a maximum in the early morning and a minimum in the afternoon. The outdoor radon activity averages corresponding to the different sessions are 20.42, 14.50 and 29.58 $Bq.m^{-3}$ for morning, afternoon and evening, respectively. Data obtained are in good agreement with each other authors [21, 22]. It can be explained mainly by the variation of the atmospheric stability affected by the time variations and spatial differences in the temperature of the ground and surface air as a result of the solar radiation flux. There are regular periodic changes in the atmospheric stability that are caused by the solar heating of the soil surface which in turn causes heating of the near-surface atmosphere. During the day, the temperature increases and temperature differences come into being due to solar radiation. The surface air circulates in a thermo-convective motion and therefore radon and radon progeny get dispersed vertically in a thick air layer. After sunset the surface air layer cools down and temperature differences decrease, which cause an increase in the atmospheric stability (thermo-convective motion weakens); so radon and radon progeny accumulate near the surface. Since the temperature reaches its maximum in the afternoon and minimum in the early morning, radon and radon progeny concentrations are low in the afternoon and high in the early morning [23].

Fig. 5 shows the negative correlation between temperature and outdoor radon activity, which is approximately exponential with a correlation coefficient of R^2=0.65. As shown in Fig. 6, the correlation between relative humidity and outdoor radon activity is also approximately exponential but positive, with a correlation coefficient of R^2=0.49. This is due to the fact that as temperature increases, the relative humidity decreases resulting in the decrease of moisture content in the atmosphere.

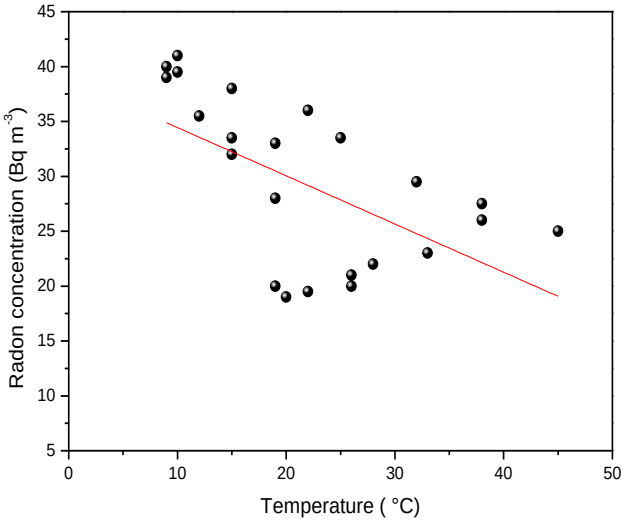

Fig. 5. Correlation between outdoor radon concentration and temperature.

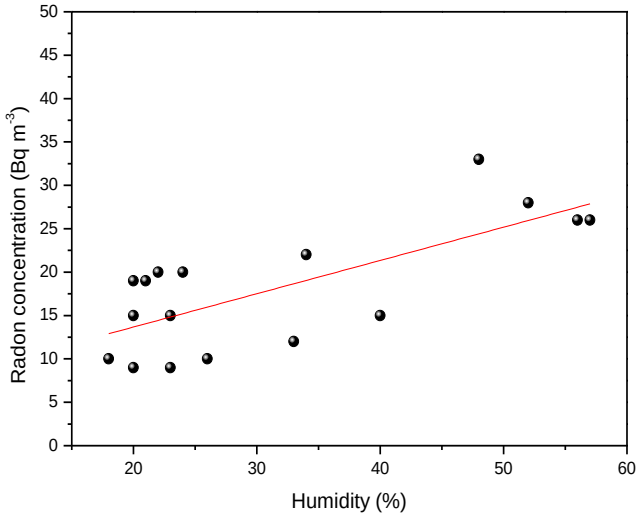

Fig. 6. Correlation between outdoor radon concentration and relative humidity

VI. CONCLUSION

In this paper, a 3D CFD model was developed to investigate the transport and distribution of radon concentrations in the atmosphere. Using this model one can evaluate the concentration of radon and their progenies in the outdoor atmosphere. The measured atmospheric concentration of radon and its progeny in Beni-Mellal city reach a maximum value in the morning. The stable atmosphere during the night helps more accumulation of radon and hence, the night time concentrations are higher than the daytime atmospheric concentrations of radon. The concentrations are the lowest in the afternoon, when the atmosphere is unstable. A correlation between radon concentration and relative humidity, and the negative correlation with temperature air is observed. The results obtained by CFD model have been agreement with those obtained experimentally.

REFERENCES

[1] UNSCEAR 2000. Sources and effects of ionizing radiation. United Nations scientific committee on the effects of atomic radiation, New York, United Nation.

[2] P. Ravikumar, and R.K. Somashekar, ‘’Determination of the radiation dose due to radon ingestion and inhalation’’. *Inter J of Enviro Sci and Tech.*, vol. 11, pp. 493–508 (2014).

[3] R.K.S. Pruthvi, M.S. Chandrashekara, and L. Paramesh, ‘’Studies on spatial variations of radon and its progeny inside a dwelling, Mysore city, India’’. *Geography Physics*., vol. 3, pp. 234-237 (2014).

[4] J. Cheng, Q. Guo, and T. Ren, ‘’Radon Levels in China’’. *J of Nuclear Science and Technology*. vol. 39, pp. 695–699 (2002).

[5] C.B. Adriana, ‘’Radon and thoron progeny concentration variability in relation to meteorological conditions at Bucharest (Romania)’’. *J of Env Radio*., vol. 83, pp. 171–189 (2005).

[6] X. Dong, W. Hanqing, and J.K. Kimberlee, ‘’Radon dispersion modeling and dose assessment for uranium mine ventilation shaft exhausts under neutral atmospheric stability’’. *J of Envi Radio,*, vol. 129, pp. 57–62 (2014).

[7] R. Rabi, and L. Oufni, ‘’Study of radon dispersion in typical dwelling using CFD modeling combined with passive-active measurements’’. *Radiat Phys Chem.*, vol. 139, pp. 40-48 (2017).

[8] J.F. Vinuesa, and S. Galmarini, ‘’Characterization of the ^{222}Rn family turbulent transport in the convective atmospheric boundary layer’’, *Atmos Chem Phys.*, vol. 7, pp 697–712 (2007).

[9] K.A. Vinod, V. Sitaraman, R.B. Oza, and T.M. Krishnamoorthy, ‘’Application of a numerical model for the planetary boundary layer to the vertical distribution of radon and its daughter products’’. *Atmos Enviro*., vol. 33, pp. 4717–4726 (1999).

[10] N. Yuichi, K. Takahiro and Y. Keiko, ‘’Radon inhalation suppresses nephropathy in streptozotocin-induced type-1 diabetic mice’’. *J of Nuclear Science and Technology*, vol. 53, pp. 909–915 (2016).

[11] R. Rabi, and L. Oufni, ‘’Evaluation of indoor radon equilibrium factor using CFD modeling and resulting annual effective dose’’. *Radiat Phys and Chem.*, vol. 145, pp. 213–221 (2018).

[12] L. Oufni, M.A. Misdaq, and M. Amrane, ‘’Radon level and radon effective dose rate determination in Moroccan dwellings using SSNTDs’’. *Radiat Meas.*, vol. 40, pp. 118-123 (2005).

[13] M.A. Misdaq, M. Amrane, and J. Ouguidi, ‘’Concentrations of ^{222}Rn, ^{220}Rn and their decay products measured in outdoor air in various rural zones (Morocco) by using solid-state nuclear track

detectors and resulting radiation dose to the rural populations''. *Radiat Protec Dosim.*, vol. 138, pp. 223–236 (2010).

[14] L. Oufni, and M.A. Misdaq, ''Radon emanation in a limestone cave using CR-39 and LR-115 solid state nuclear track detectors''. *J Radioanal Nucl Chem.* vol. 250, pp. 309–313 (2001).

[15] J.M. Stajic, B. Milenkovic, and D. Nikezic, ''Study of CR-39 and Makrofol efficiency for radon measurements''. *Radiat Meas.*, vol. 117, pp. 19-23 (2018).

[16] W.P. Jones, and B.E. Lander, ''The calculation of low- Reynolds number phenomena with a two-equation model of turbulence''. *Inte. J. of Heat and Mass Transfer*, vol. 16, pp. 1119–1130 (1973).

[17] Y. Yongjun, K. Long, Q.Z. Chung, and J.K. Kimberlee,'' Evaluation of ^{222}Rn and ^{220}Rn discriminating concentration measurements with pinhole-based twin cup dosimeters using computational fluid dynamics simulations''. *Radiat Meas.* (2020).

[18] R. Haxaire, ''Caractérisation et Modélisation des écoulements d'air dans une serre'', PhD Thesis, Université de Nice, Sophia Antipolis, France, vol. 148, (1999).

[19] H. Majdoubi, T. Boulard, H. Fatnassi, and L. Bouirden, ''Airflow and microclimate patterns in a one-hectare Canary type greenhouse: An experimental and CFD assisted study''. *Agricul Forest Meteo*., vol. 149, pp. 1050–1062 (2009).

[20] K. Sun, Q. Guo, and W. Zhuo, ''Feasibility for Mapping Radon Exhalation Rate from Soil in China''. *Journal of Nuclear Science and Technology*, vol. 41, pp. 86–90 (2003).

[21] A.C. Baciu, ''Radon and thoron progeny concentration variability in relation to metrological conditions in Bucharest (Romania)''. *J Environm Radioact.*, vol. 83, pp. 171–189 (2005).

[22] K. Sun, Q. Guo, and J. Cheng, ''The Effect of Some Soil Characteristics on Soil Radon Concentration and Radon Exhalation from Soil Surface''. *Journal of Nuclear Science and Technology*, vol. 41, pp. 1113–1117 (2004).

[23] M. Amrane, L. Oufni, B. Manaut, and S. Taj, ''Measurements of ^{222}Rn, ^{220}Rn and Their Decay Products in the Environmental Air of the Errachidia Area (Morocco) Using SSNTDs''. *Ener and Envir Engineering* , vol. 1, pp. 62–67 (2013).

Nomenclature

C radon concentration (Bq m^{-3})

ρ air density (Kg m^{-3})

u_i velocity components in x, y, and z coordinates (m s^{-1})

x_i the coordinate axis in the direction i (i = 0, 1, 2)

P pressure difference (N m^{-2})

μ molecular viscosity (N s m^{-2})

μ_t turbulent viscosity (N s m^{-2})

g gravitational acceleration (m^2 s^{-1})

k energy kinetic turbulent (m^2 s-2)

ε dissipation of turbulent kinetic energy (m^2 s^{-2})

D_e effective radon diffusion (m^2 s^{-1})

ϵ effective porosity

λ is the radon decay constant (s^{-1})

ρ_s is the dry bulk density (Kg m^{-3})

f radon emanation coefficient

$A_c(^{226}\mathrm{Ra})$ α-activities of radium ($\mathrm{Bqkg^{-1}}$)

$A_c(^{232}\mathrm{Th})$ α-activities of thorium ($\mathrm{Bqkg^{-1}}$)

D_G^{LR} and D_G^{CR} are the track density ($\mathrm{tracks\ cm^{-2}s^{-1}}$)

E_0 radon exhalation rate ($\mathrm{Bqm^{-2}h^{-1}}$)